Surface & Coatings Technology 260 (2014) 417–423

Contents lists available at ScienceDirect

Surface & Coatings Technology

journal homepage: www.elsevier.com/locate/surfcoat

Modelling of laser ablation and reactive oxygen plasmas for pulsed laser deposition of zinc oxide

S. Rajendiran [a], A.K. Rossall [a], A. Gibson [b], E. Wagenaars [a,*]

[a] York Plasma Institute, Department of Physics, University of York, York YO10 5DD, UK
[b] Centre for Plasma Physics, School of Mathematics and Physics, Queen's University Belfast, Belfast BT7 1NN, UK

ARTICLE INFO

Available online 22 July 2014

Keywords:
Pulsed laser deposition
Inductively coupled plasma
Oxygen radio-frequency plasma
Zinc oxide thin film

ABSTRACT

Pulsed laser deposition (PLD) in a low-pressure oxygen atmosphere is commonly used for the production of high-quality, stoichiometric zinc oxide thin films. An alternative approach that has the potential benefit of increased process control is plasma-enhanced PLD, i.e. the use of a low-temperature oxygen plasma instead of a neutral gas. So far, the development of PE-PLD, and PLD in general, has been hampered by a lack of detailed understanding of the underpinning physics and chemistry. In this paper, we present modelling investigations aimed at further developing such understanding. Two-dimensional modelling of an inductively-coupled radio-frequency oxygen plasma showed that densities of 10^{14}–10^{15} cm^{-3} of reactive oxygen species O and O_2^* can be produced for operating pressures between 3 and 100 Pa. Together with the absolute densities of species, also the ratio between different reactive species, e.g. O and O_2^*, can be controlled by changing the operating pressure. Both can be used to find the optimum conditions for stoichiometric zinc oxide thin film deposition. Additionally, we investigated laser ablation of zinc using a different two-dimensional hydrodynamic code (POLLUX). This showed that the amount of material that is ablated increases from 2.9 to 4.7 μg per pulse for laser fluences from 2 to 10 J/cm^2. However, the increased laser fluence also results in an increased average ionisation of the plasma plume, from 3.4 to 5.6 over the same fluence range, which is likely to influence the chemistry near the deposition substrate and consequently the film quality.

1. Introduction

The last decade has seen a significant expansion of research into zinc oxide (ZnO) films. ZnO is a direct band gap II–VI semiconductor with unique optical and electronic properties that can be applied in a variety of applications, e.g. as transparent electrodes in liquid crystal displays and photovoltaics, and as thin-film transistors and light-emitting diodes in microelectronics [1–3].

Controlled fabrication of high-quality thin films of ZnO is challenging. Because of its high melting temperature (~2000 °C), thermal evaporation of ZnO is impractical and alternative, more complex techniques are required. Techniques such as chemical vapour deposition (CVD), molecular beam epitaxy (MBE), magnetron plasma sputtering, and pulsed laser deposition (PLD) have all successfully been applied to fabricate ZnO films with properties desired for certain applications [4]. The PLD technique offers the advantage of high deposition rates, (limited) control of stoichiometry and easy interchange of materials. The main disadvantages are the limited area of deposition and possible incorporation of macroscopic particles in the films, generated during laser ablation. Also, as for most ZnO deposition techniques, fabrication of high-quality films relies heavily on empirical methods to find the optimal growing conditions for the desired film properties. There is a distinct lack of understanding of the science underpinning these deposition techniques [5]. For example, in PLD stoichiometric transfer from the target to the film is often not achieved in practice due to different sticking coefficients and re-sputtering of the different species. Also, control of the crystal structure of the deposited film is often lacking.

Adding a background atmosphere of oxygen gas has proven to allow additional control over the film's oxygen content and also crystallisation structure [6,7]. The plasma plume from the laser ablation travels through, and interacts with, the oxygen background gas, before it is deposited on the substrate. The interactions between the plume and the background gas molecules are complex but will include electron-collision induced dissociation of the oxygen molecules into highly reactive oxygen atoms that are subsequently deposited on the target or interact with the already deposited film, increasing the oxygen content of the film to the desired value. Unfortunately, there is a lack of control parameters for stoichiometry in this system with oxygen pressure being one of very few in this highly complex system.

An alternative approach is plasma-enhanced PLD (PE-PLD) in which a low-temperature, reactive oxygen plasma background is introduced instead of a neutral gas. In this way, we de-couple the creation of

* Corresponding auhtor at: York Plasma Institute, Department of Physics, University of York, York, YO10 5DD, UK.
E-mail address: erik.wagenaars@york.ac.uk (E. Wagenaars).

http://dx.doi.org/10.1016/j.surfcoat.2014.06.062

reactive oxygen species from the interaction with the ablation plume. The background plasma independently creates a mix of highly reactive neutral oxygen atoms and molecules, positive and negative ions and neutral gas. Moreover, this reactive oxygen environment is also present between laser pulses, allowing surface preparation and restructuring between deposition pulses. Importantly, the operating conditions of this plasma, i.e. pressure, power, bias, discharge geometry, will determine the amount and types of the different reactive species and can hence be optimised for stoichiometry control and crystal structure growth of the film. Such an approach has been investigated by several groups. Huang et al., used a radio-frequency (rf) parallel plate discharge in 3–40 Pa oxygen as a PLD background and observed a ZnO film with the preferred (0 0 2) *c*-axis orientation and a reduction in the film's defects and a higher deposition rate compared to traditional PLD [8]. Scarisoreanu et al. used a separate rf oxygen plasma source. This plasma expands as a directional beam into the PLD deposition chamber onto the substrate. They found that they could fabricate films with different crystalline orientations by changing the relative orientation of the oxygen plasma beam, ablation plasma and substrate [9]. Nistor et al. reports growth of both good quality *a*-axis and *c*-axis ZnO films by using PLD with a directional rf plasma beam under different orientations [10]. In all these studies the focus was on the resulting films; the oxygen plasma properties were not measured (or modelled) and optimised empirically.

In this paper, we present modelling results of a new oxygen plasma source for plasma-enhanced PLD of ZnO films. This source is based on the well-characterised Gaseous Electronics Conference (GEC) reference cell [11,12] and allows us to accurately characterise the types and concentrations of reactive oxygen species that are produced and play a role in the thin film deposition process. We present a modelling study of this discharge, focussing on the variation of the different reactive species at a deposition substrate as a function of the oxygen input pressure. Additionally, we present results from a laser ablation model showing how laser parameters are available for control of the content of the plasma plume that will be interacting with the oxygen plasma environment. The overall goal of this research is to provide a better understanding of the underlying plasma physics in PLD and PE-PLD processes, leading to a better control of the deposition process and film quality.

2. Description of models

2.1. Reactive oxygen plasma model

We used the Quantemol-VT software [13] to calculate the plasma characteristics of an inductively coupled rf oxygen plasma. Quantemol-VT builds upon the comprehensively validated Hybrid Plasma Equipment Model (HPEM) developed by Kushner et al. Detailed information about HPEM can be found in [14]. In short, the plasma properties are calculated in three steps. First, Maxwell's equations are solved to calculate the electromagnetic fields within the discharge volume. Based on these fields, the electron energy distribution function, and electron impact reaction rates are calculated using a Boltzmann solver. Subsequently, the reaction rates are used to determine the various oxygen species and electron density distributions and Poisson's equation for the electrostatic field. The calculation loop is closed by using the electrostatic field for the calculation of the electromagnetic fields. This self-consistent cycle is iterated until convergence.

An important part of the model is the plasma chemistry, i.e. the species and reactions that are included in the model. For this we followed the species and reaction set used by Tinck and Bogaerts [15] for an O_2 inductively coupled plasma for plasma enhanced atomic layer deposition. This includes electrons and nine different oxygen species, i.e. O_2, $O_2(v)$, O_2^*, $O_2^*(1S)$, O_2^+, O, O*, O^+, O^-. Here $O_2(v)$ is a vibrationally excited state of O_2, O_2^* is the $O_2(^1\Delta)$ state and $O_2^*(1S)$ refers to the $O_2(^1\Sigma)$ state of molecular oxygen. O* is the O(1D) state of atomic oxygen. Following Tinck and Bogaerts [15], we do not include O_2^- and O_3 in our model since these are believed to be of minor importance for these types of plasmas. A total of 50 reactions are included, as specified in [15]. The rates for the electron impact reactions are calculated using cross sections from Phelps et al. [16]. The reaction rates for the heavy particle reactions are taken from [15]. At the walls of the reactor, all the O_2^+, O^- and O^+ ions are considered to be neutralised and reflected back into the plasma. O*, $O_2^*(1S)$, $O_2(v)$, O_2^* are de-excited to the ground state in a wall collision and reflected back into the plasma, with reaction probabilities of 1.00 for O*, 0.02 for $O_2^*(1S)$, 0.2 for $O_2(v)$, and 0.007 for O_2^* [17,18]. Atomic oxygen, O, is assumed to recombine at the wall to form O_2 with a reaction rate of 0.2 [19].

The discharge geometry is schematically shown in Fig. 1. It is based on the inductively coupled plasma (ICP) version of the rf GEC reference cell [11,12]. This is a widely used, well-characterised experimental platform for comparing plasma measurements in a common reactor, aimed at gaining insight in the rf discharge behaviour. As can be seen in Fig. 1, the plasma consists of a vacuum chamber with a copper five-turn planar coil antenna and metal electrode. Electrical power from the antenna is inductively coupled into the plasma volume through the bottom of a quartz cylinder (4 mm thickness, 140 mm diameter). The lower electrode is made of stainless steel and has a diameter of 100 mm. It can be electrically biased but was grounded for these simulations. The distance between the electrode and the quartz cylinder is 40 mm. The coil antenna is driven with a sinusoidal rf voltage at 13.56 MHz. The power to the coil was set at 400 W for our simulations. The discharge volume is filled with oxygen gas at pressures varying from 3 to 100 Pa.

2.2. Laser ablation model

In laser ablation, a high-power, pulsed laser interacts with a solid target material, removing the surface layer of the target and turning it into an expanding plasma plume. We use a dedicated two-dimensional Eulerian hydrodynamic code called POLLUX to study the laser ablation process. The POLLUX code was developed by Pert et al. and further details can be found in [20,21]. In short, the code solves the three first-order quasi-linear partial differential equations of hydrodynamic flow. The laser energy absorption in both the solid, leading to melting and vaporisation, and the plasma plume, leading to plasma heating via inverse bremsstrahlung, are included. A CHART-D [22] equation of state (EOS) is used for the calculation of the phase and phase boundaries of the target during the ablation process. The ionisation in the plasma plume is determined using the Thomas–Fermi model [23]. The code assumes a cylindrical symmetric geometry, with the target and the region

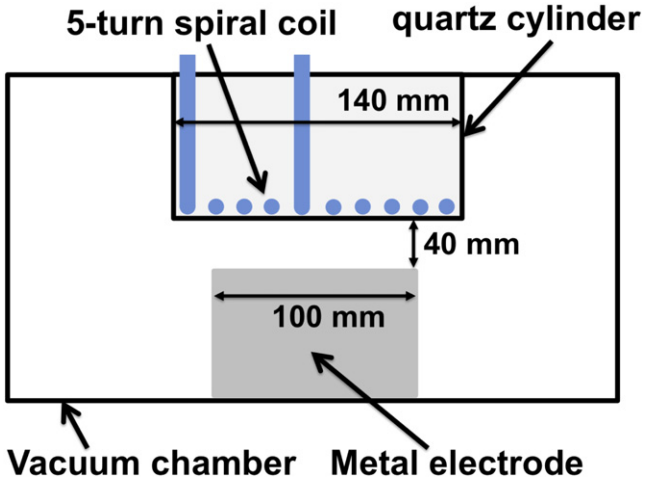

Fig. 1. Schematic diagram of the inductively coupled plasma source under study. The reactor is cylindrically symmetric and consists of a stainless steel vacuum chamber, a 5-turn coil antenna inside a quartz cylinder, and a metal electrode. The design is based on the GEC rf reference cell [11,12].

above the surface represented by a two-dimensional mesh aligned along the laser direction. In the rising edge of the laser pulse, the energy will be mainly absorbed in the cells at the target surface, leading to melting and plasma formation. This expanding plasma is then heated further by the remainder of the incoming laser via inverse bremsstrahlung absorption.

In this paper, we focus our attention on the ablation of pure Zn targets by a UV pulsed laser, which is directly relevant for PLD. We simulate the interaction of a Zn target with a 355 nm laser pulse with a FWHM duration of 5 ns and a FWHM focussed beam diameter of 2.0 mm. The laser fluence is varied between 2 and 10 J cm^{-2}.

3. Results and discussion

3.1. Reactive oxygen plasma

Fig. 2 contains results of the reactive oxygen plasma model, showing 2D maps of the species density distributions for an oxygen discharge at 5 Pa and 400 W rf input power.

It can be seen from the charged particle (electron, O^-, O_2^+, O^+) distributions that the main power dissipation happens in front of the quartz cylinder, just below the coil. The dominant positive ion is O_2^+ with a density in the order of 2×10^{11} cm^{-3}. The O^+ densities are almost an order or magnitude lower. Also, this is an electronegative plasma since there is a significant number of negative ions, i.e. O^-. The value for the O^- density is of the same order as the electron density, giving a reactor-averaged electronegativity of about 0.5.

The neutral species, O, O_2^*, $O_2^*(1S)$, O^*, and $O_2(v)$ have peak densities which are 2–3 orders of magnitude higher than the charged particle densities. Also, the distribution of the neutral species is far more homogenous across the inter-electrode gap. It is likely that for applications in the area of plasma-enhanced PLD, the effect of these reactive neutral species will be dominant over the charged particles. Especially when a PLD-substrate material is placed on, or close to, the bottom electrode, the difference in density between the charged and neutral species is more than 3 orders of magnitude, emphasising the importance of the neutral, reactive species. It is known that atomic oxygen (O) and singlet

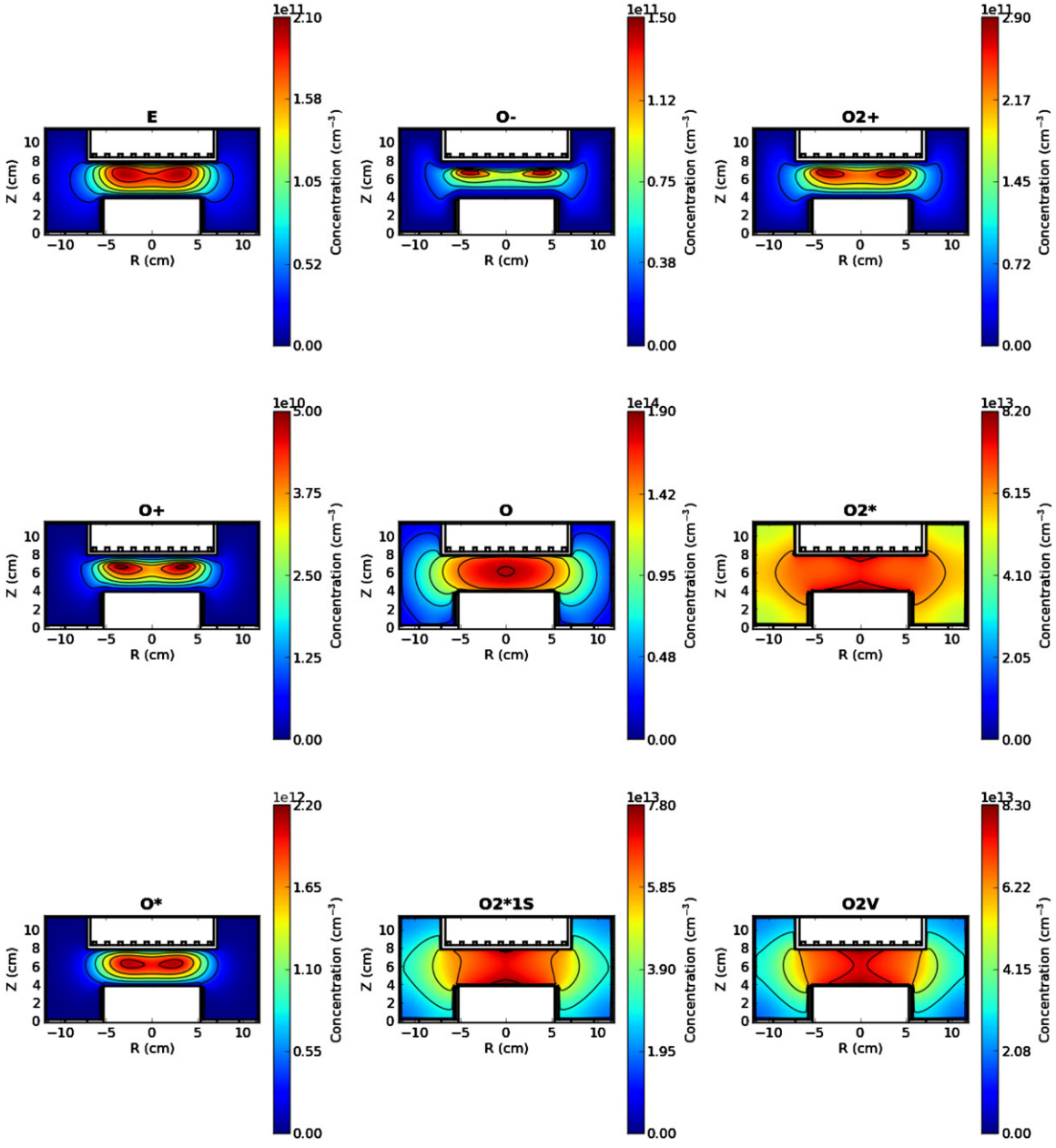

Fig. 2. Results of the reactive oxygen plasma model. Plotted are the densities of the different species for a discharge in 5 Pa oxygen gas with 400 W input power.

delta oxygen ($O_2(^1\Delta)$, called O_2^* in our model) are chemically highly reactive and it is likely that these species play an important role in the deposition process in PLD with an O_2 gas background. In the case of an O_2 gas background, the reactive O and O_2^* species are created by reactions between the expanding plasma plume and background gas. Therefore, the amount of reactive oxygen species is directly coupled to the ablation process, limiting control of the properties of the reactive oxygen densities. Using a separate rf plasma source to provide the reactive oxygen species gives additional control over the densities and distributions, and hence the film deposition process.

As an illustration we have varied the O_2 pressure in our rf plasma to 50 Pa. The results of these simulations are shown in Fig. 3, again presenting the species density distributions for an oxygen discharge at 400 W rf input power. Compared to the 5 Pa case, the charged species are even more localised in a doughnut shape in front of the quartz cylinder. Interestingly, the peak densities of the charged species are very similar to those of the 5 Pa case and the reactor-averaged density is lower by about a factor of 3 for all charged species. On the other hand the reactive neutral species show both higher peak and reactor-averaged densities, a factor 3 for O and 6 for O_2^*. However, especially for O (and $O_2^*(1S)$ and $O_2(v)$) the distribution across the reactor is no longer homogenous; it is localised in the same place as the charged species. These differences in densities with pressure can be exploited to optimise required oxygen content during the PLD process.

To further investigate these possibilities, we varied the pressure between 3 and 100 Pa and monitored the density of O and O_2^* at a position in front of the centre of the metal electrode since this is a good position to place a deposition substrate. The results, shown in Fig. 4, indicate that the O_2^* density increases with pressure from 4×10^{13} cm^{-3} at 3 Pa to 1×10^{15} cm^{-3} at 100 Pa, which roughly scales with the O_2 gas pressure. O on the other hand shows a different behaviour with pressure. It only varies between 3×10^{13} cm^{-3} and 2×10^{14} cm^{-3}, with the highest density at 10 Pa and the lowest at 100 Pa. The trend above 10 Pa is opposite to that of O_2^*, i.e. decreasing density with pressure for O while it is increasing for O_2^*. This gives an interesting range of operating conditions in which the relative density of 2 main reactive species can be altered significantly. At 3 Pa, O is the dominant species, with a density twice that of O_2^*. By increasing the pressure, the dominant reactive species can be changed to O_2^*, with a density 35 times higher than that of O at 100 Pa. This change in the type of reactive oxygen species can have an influence on the deposited thin film properties, depending on the exact chemistry of the PLD deposition process. Such an effect would be similar to what Blackwell et al. observed in their molecular dynamics and on-the-fly kinetic Monte Carlo simulations

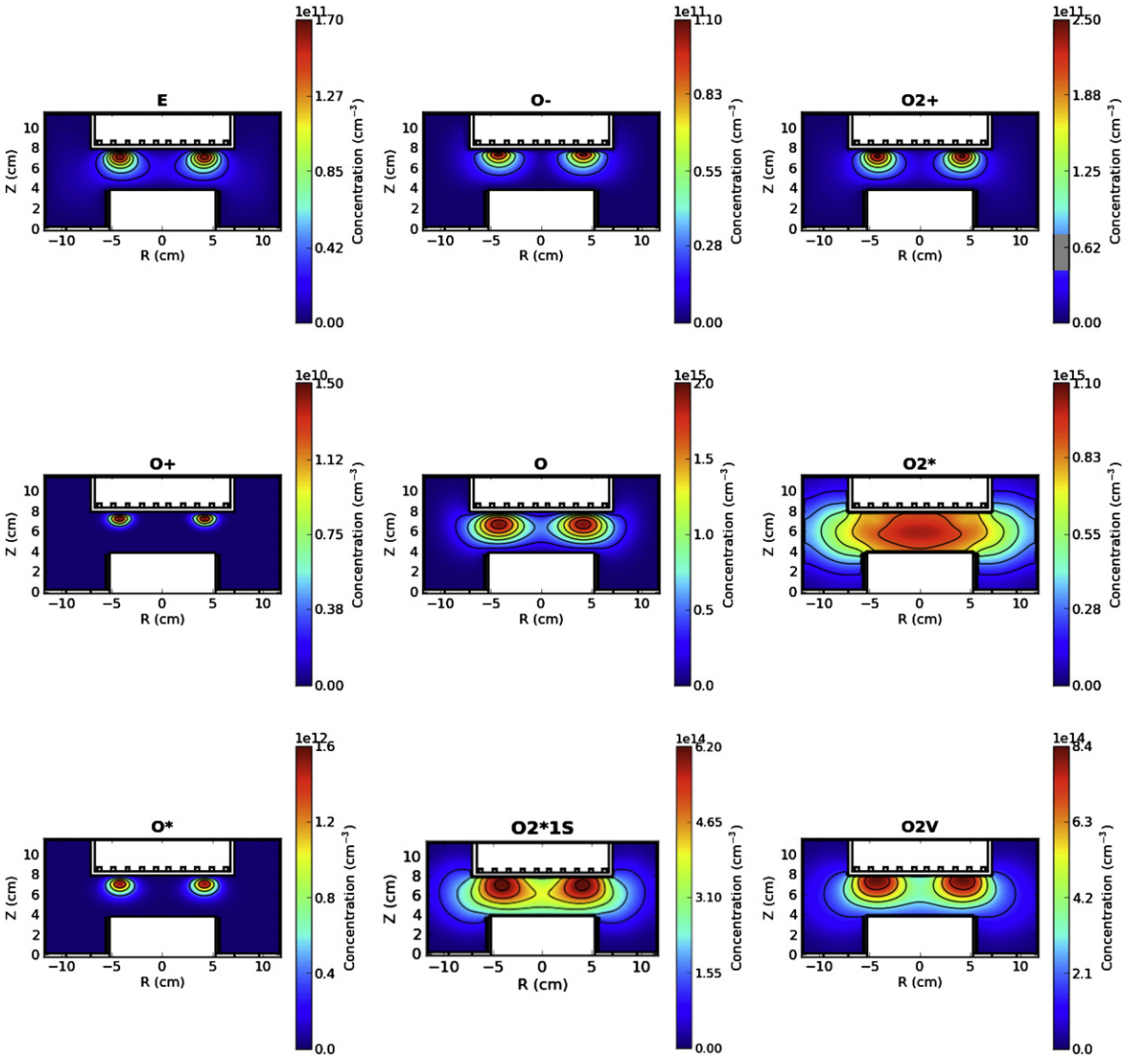

Fig. 3. Results of the reactive oxygen plasma model. Plotted are the densities of the different species for a discharge in 50 Pa oxygen gas with 400 W input power.

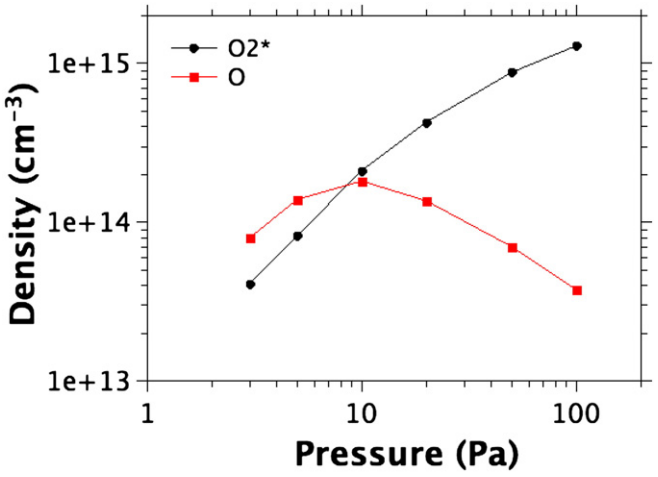

Fig. 4. Modelled densities of O and O_2* at a position in front of the centre of the metal electrode as a function of pressure.

[24]. They found that the O/O_2 ratio influenced the stoichiometry, crystal structure and quality of the deposited ZnO films [24].

3.2. Laser ablation model

Fig. 5 shows results from the laser ablation model for a laser fluence of 6 J/cm^2, 5 ns pulse duration and 2 mm diameter focal spot. Plotted are the axial velocity and temperature profiles along the symmetry axis of the ablation plume (i.e. perpendicular to the target, through the centre of the laser spot). It can be seen that the relatively short (5 ns) laser pulse ablates some material which moves away from the target surface with a velocity of 4×10^4 m/s with the highest velocities near the front of the expanding plume. The electron temperature in this plume is between 12 and 18 eV. After 50 ns, the plume has expanded over a distance of about 1.7 mm from the original target surface, with the axial velocity decreasing slightly to 3×10^4 m/s. Since at this point in time the entire laser pulse has passed, there is no new material being ejected from the target as shown by the axial velocity of nearly zero at the target surface. This shows that during a single laser pulse, all the material is ablated during the first 50–100 ns, which means that in a PLD process the deposition is likely to be pulsed as well since typical laser repetition rates are 10–50 Hz. The pulsed nature of the laser ablation process is also clear from Fig. 6, which shows a 2D map of the simulated electron density at a time of 40 ns after the start of the laser pulse. Electron densities of up to 2×10^{20} cm^{-3} are observed near the front of the plasma plume. The shape of the plasma plume shows that there is a relatively narrow, high-density plasma front moving away from the laser interaction point. Behind this there is a plasma of lower density ($5–10 \times 10^{19}$ cm^{-3}). Close to the target surface (<0.5 mm) the electron density is high, but this region of plasma has very low velocities, which means that it will not take part in the deposition process, several centimetres from the target surface. Nevertheless, depending on the repetition rate of the laser, it can have an effect on the ablation process of the subsequent laser pulse since subsequent pulses will interact with a plasma surface rather than a solid surface. However, it should be noted that even for simulations with a solid target, the majority of the laser energy absorption is through inverse bremsstrahlung in the plasma plume, not direct heating of the solid target.

One of the parameters that can be used to control a PLD process is the laser fluence. Fig. 7 shows the total mass of the expanding plasma plume, and the average ionisation degree (i.e. the average number of bound electrons that is removed from every atom) of the plume after a single 5 ns pulse with different laser fluences. The simulations show that we can control the amount of material that is ablated per pulse by changing the laser fluence, i.e. an increase from 2.9 to 4.7 μg per pulse for laser fluences from 2 to 10 J/cm^2. Interestingly, it is not only the amount of material that is affected by the laser fluence, but also the composition of the plume. The average ionisation increases from 3.4 to 5.6 over the same range of fluences. This implies that the plasma ions at high fluences are more highly ionised than at low fluences, possibly affecting the chemistry of the deposition process. It highlights the complexity and interdependency of the control parameters of a PLD process, e.g. increasing the laser fluence will not only increase the amount of ablated material (and therefore the film deposition rate), it will at the same time change the ionisation degree and therefore deposition chemistry and film properties. Nevertheless, modelling studies like ours can help to highlight and understand these dependencies so that effective control of a PLD process can be achieved.

Finally, traditional ZnO PLD is performed by ablating a ZnO target in a low-pressure oxygen atmosphere. The addition of the inductively coupled plasma dramatically increases the amount of reactive oxygen species, opening up the possibility of completely decoupling the Zn and O sources for a ZnO film, i.e laser ablation of pure zinc in combination with oxygen species from an ICP source. In other words, laser ablation of pure zinc in combination with oxygen species from an ICP source. Our simulations show that in a single laser pulse about 1×10^{17} Zn ions are formed. When this plume expands towards a substrate, about 5 cm away, the typical density at the substrate will be in the order of 10^{14} cm^{-3}. The oxygen ion density is typically only 10^{11} cm^{-3}, however, the densities at a substrate surface of *neutral* reactive oxygen species, e.g. O and O_2^*, are in

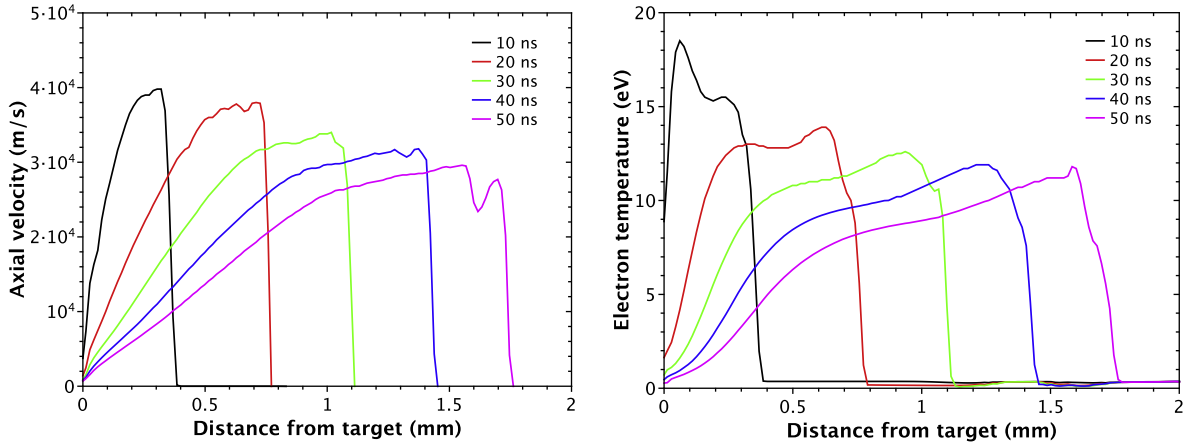

Fig. 5. Simulated axial velocity (left) and electron temperature (right) profiles for different times after the start of the 5 ns laser pulse. The laser fluence was 6 J/cm^2 and the target material was zinc.

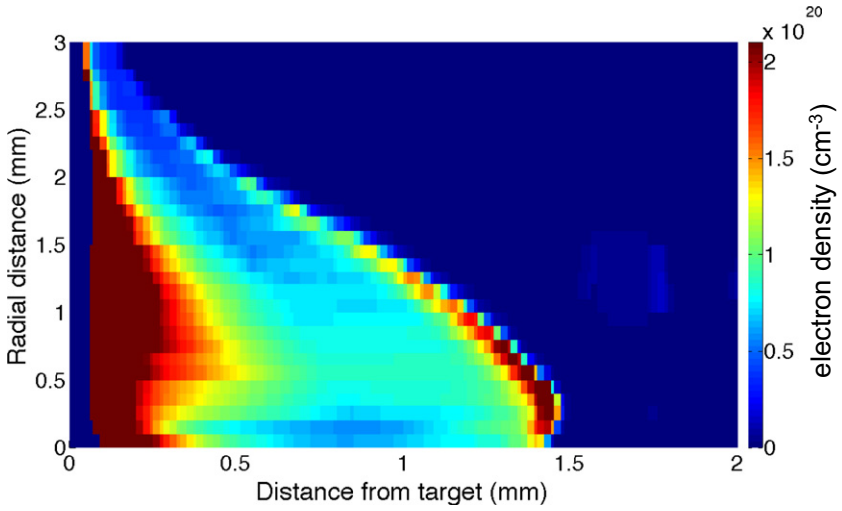

Fig. 6. Results of the cylindrically symmetric laser ablation simulation showing a 2D map of electron density at a time of 40 ns after the start of the laser pulse (6 J/cm^2, 1 mm radius focal spot, zinc target).

the order of 10^{14} cm^{-3}, like the Zn ions. Therefore, the ratio of reactive Zn to reactive oxygen in front of the substrate will be close to unity. Furthermore, the absolute values of these densities are very comparable to the densities found in other plasma-based ZnO deposition techniques, e.g. magnetron plasma sputtering, where operating pressures of 0.1–1.0 Pa are used and ionisation is believed to be close to 100%, leading to particle densities of 10^{13}–10^{14} cm^{-3} [1,25,26]. In PE-PLD we can have equal densities of Zn and oxygen arriving at a substrate so we could envisage deposition of a good quality ZnO film with reasonable stoichiometry. Also, the fact that the absolute value of the particle densities in our PE-PLD technique are similar to those observed in traditional high-quality ZnO deposition methods, is encouraging for the feasibility of our proposed technique. The prospect of depositing ZnO films from separate Zn and O sources is interesting, especially from a process control point of view.

4. Conclusion and outlook

In this paper we present results from two different numerical models, investigating different aspects of (plasma-enhanced) PLD of ZnO thin films. Modelling of the laser ablation of zinc shows that in a typical PLD ablation pulse a few micrograms of material per pulse is ablated. The amount of material per pulse can be controlled with the laser fluence, however the average ionisation is also affected, which can change the subsequent deposition dynamics. Therefore, one has to be cautious when using the laser fluence as a direct PLD control parameter for deposition rate.

Secondly, we showed that using a separate inductively coupled plasma source, instead of a traditionally used oxygen gas background, can give significant amounts (5×10^{13}–10^{15} cm^{-3}) of reactive oxygen species such as O and O_2*. It is likely that these species play an important role in the film deposition process and therefore it is advantageous to be able to independently control the amount and relative ratio of reactive species such as O and O_2*.

Finally, by using an ICP source, it could be feasible to completely decouple the Zn and O sources for ZnO PLD. Laser ablation of pure zinc gives ion densities comparable to reactive oxygen densities in an ICP source. Incorporating an ICP plasma in a plasma-enhanced PLD setup offers independent control over the Zn and reactive oxygen densities, and therefore additional control over the deposition process and thin film properties. Experiments are planned for the near future to benchmark the presented simulation results and test this new deposition concept.

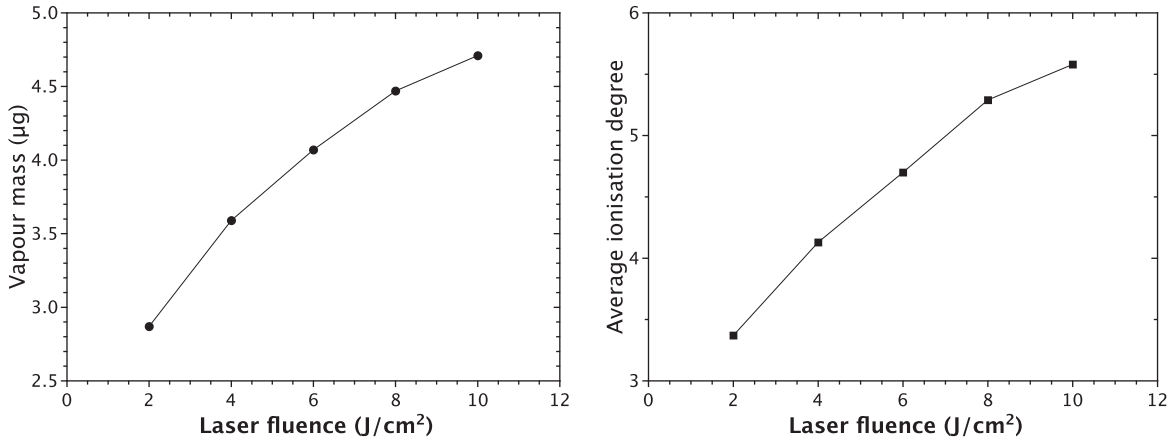

Fig. 7. Laser ablation simulations showing the total mass in the expanding plasma plume (left), and the average ionisation degree (right) for different laser fluences (2, 4, 6, 8, 10 J/cm^2).

Conflict of interest

There is no conflict of interest.

Acknowledgments

We acknowledge support from the UK Engineering and Physical Sciences Research Council (EPSRC), grant EP/K018388/1.

References

[1] Ya.I. Özgür, C. Alivov, A. Liu, M.A. Teke, S. Reshchikov, V. Dogăn, S.-J. Avrutin, H. Cho, A. Morkoc, J. Appl. Phys. 98 (2005) 041301.
[2] C. Klingshirn, Phys. Status Solidi B 244 (2007) 3027–3073.
[3] D.C. Look, Mater. Sci. Eng. B 80 (2001) 383–387.
[4] J.-J. Chen, X.-R. Deng, H. Deng, J. Mater. Sci. 48 (2013) 532–542.
[5] A. Ohtomo, A. Tsukazaki, Semicond. Sci. Technol. 20 (2005) S1–S12.
[6] M. Opel, S. Geprägs, M. Althammer, T. Brenninger, R. Gross, J. Phys. D. Appl. Phys. 47 (2014) 034002.
[7] S.S. Kim, B.-T. Lee, Thin Solid Films 446 (2004) 307–312.
[8] S.-H. Huang, Y.-C. Chou, C.-M. Chou, V.K.S. Hsiao, Appl. Surf. Sci. 226 (2013) 194–198.
[9] N. Scarisoreanu, D.G. Matei, G. Dinescu, G. Epurescu, C. Ghica, L.C. Nistor, M. Dinescu, Appl. Surf. Sci. 247 (2005) 518–525.
[10] L.C. Nistor, C. Ghica, D. Matei, G. Dinescu, M. Dinescu, G. Van Tendeloo, J. Cryst. Growth 277 (2005) 26–31.
[11] P.J. Hargis Jr., K.E. Greenberg, P.A. Miller, J.B. Gerardo, J.R. Torczynski, M.E. Riley, G.A. Hebner, J.R. Roberts, J.K. Olthoff, J.R. Whetstone, R.J. Van Brunt, M.A. Sobolewski, H. M. Anderson, M.P. Splichal, J.L. Mock, P. Bletzinger, A. Garscadden, R.A. Gottscho, G. Selwyn, M. Dalvie, J.E. Heidenreich, Jeffery W. Butterbaugh, M.L. Brake, M.L. Passow, J. Pender, A. Lujan, M.E. Elta, D.B. Graves, H.H. Sawin, M.J. Kushner, J.T. Verdeyen, R. Horwath, T.R. Turner, Rev. Sci. Instrum. 65 (1994) 140–154.
[12] P.A. Miller, G.A. Hebner, K.E. Greenberg, P.D. Pochan, B.P. Aragon, J. Res. Nat. Inst. Stand. Technol. 100 (1995) 427–439.
[13] www.quantemol.com/products/quantemol-vt/ (Quantemol Ltd., London, United Kingdom).
[14] M.J. Kushner, J. Phys. D. Appl. Phys. 42 (2009) 194013.
[15] S. Tinck, A. Bogaerts, Plasma Sources Sci. Technol. 20 (2011) 015008.
[16] A.V. Phelps, JILA data center report, 28 (1985) 1.
[17] D.S. Stafford, M.J. Kushner, J. Appl. Phys. 96 (2004) 2451–2465.
[18] J.T. Gudmundsson, I.G. Kouznetsov, K.K. Patel, M.A. Lieberman, J. Phys. D. Appl. Phys. 34 (2001) 1100–1109.
[19] S. Gomez, P.G. Steen, W.G. Graham, Appl. Phys. Lett. 81 (2002) 19–21.
[20] M.S. Qaisar, G.J. Pert, J. Appl. Phys. 94 (2003) 1468–1477.
[21] G.J. Pert, J. Plasma Phys. 41 (1989) 263.
[22] S.L. Thomson, H.S. Lauson, Improvements in the Chart-D radiation hydrodynamic code, Sandia Labs Reports SC-RR-71 0714, 1972.
[23] R. Latter, Phys. Rev. 99 (1955) 1854.
[24] S. Blackwell, R. Smith, S.D. Kenny, J.M. Walls, C.F. Sanz-Navarro, J. Phys. Condens. Matter 25 (2013) 135002.
[25] R. Cebulla, R. Wendt, K. Ellmer, J. Appl. Phys. 83 (1998) 1087.
[26] J. Jie, A. Morita, H. Shirai, J. Appl. Phys. 108 (2010) 033521.